

# Realization of a Tunable 455.5-nm Laser With Low Intensity Noise by Intracavity Frequency-Doubled Ti:Sapphire Laser

Fengqin Li, Huijuan Li, and Huadong Lu

**Abstract**—A tunable single-frequency 455.5-nm laser with low intensity noise by means of intracavity frequency-doubled Ti:sapphire (Ti:S) laser is presented. By optimizing the curvature radii of the resonator mirrors, the beam waist of the fundamental wave at the Ti:S crystal is focused, and the threshold pump power is decreased, which can overcome the disadvantage of the upper threshold pump power due to the smaller gain at oscillating a wavelength of 911 nm than that of 795 nm. Based on the numerical calculation, a single-frequency 455.5-nm laser with an output power of 421 mW and an optical conversion efficiency of 3.95% is obtained from 10.65-W all-solid-state 532-nm pump laser, and the intensity noise of the 455.5 nm laser reaches the quantum noise limit at 1.8 MHz. With the obtained laser resource, the saturation absorption spectrum of the higher state excitation transition of  $^{133}\text{Cs}$  is successfully measured when its frequency is continuously scanned over 3.4 GHz.

**Index Terms**—Titanium, intracavity frequency doubled, frequency tuning, 455.5 nm laser.

## I. INTRODUCTION

CONTINUOUS-WAVE (CW) single-frequency tunable coherent laser sources in the blue spectral region are useful for applications in biomedicine, metrology, high-resolution spectroscopy, display technology, atomic-trapping, quantum optics and so on owing to their continuous frequency tuning ability across the range of interest and intrinsic merits of low intensity noise, narrow linewidth as well as the good beam quality. For instance, single-frequency 455 nm laser as seawater transparent window is applied in the ocean lidar and underwater laser communication [1]. In the atomic physics, the cooling transmission of  $^{138}\text{Ba}^{2+}$  ions falls within the wavelength of 455 nm [2]. The saturation absorption spectrum of the higher-state excitation transition  $6^2\text{S}_{1/2} \leftrightarrow 7^2\text{P}_{3/2}$  of  $^{133}\text{Cs}$  also falls within the wavelength of 455 nm [3], which can realize the further quantum manipulation

Manuscript received May 25, 2015; revised November 20, 2015; accepted December 7, 2015. Date of publication December 17, 2015; date of current version January 19, 2016. This work was supported in part by the National Natural Science Foundation of China under Grant 61405107, Grant 61227015, and Grant 61227902, in part by the Natural Science Foundation of Shanxi Province under Grant 2014021011-3, and in part by the Scientific and Technological Innovation Programs of Higher Education Institutions in Shanxi under Grant 2013104. (Corresponding author: Huadong Lu.)

The authors are with the State Key Laboratory of Quantum Optics and Quantum Optics Devices, Institute of Opto-Electronics, Shanxi University, Taiyuan 030006, China (e-mail: lfq@sxu.edu.cn; hjfriends@163.com; luhuadong@sxu.edu.cn).

Color versions of one or more of the figures in this paper are available online at <http://ieeexplore.ieee.org>.

Digital Object Identifier 10.1109/JQE.2015.2509243

from long wavelength to short wavelength [4]. In 1994, M. P. Le Flohic et al. reported CW room-temperature upconversion laser at 455 nm in a  $\text{Tm}^{3+}$  fluorozirconate fiber. However, the output power was only 3 mW [5]. In 2001, M. Schmidt et al. generated 455 nm radiation by intracavity doubling of a Nd:LiLuF<sub>4</sub> laser with the output power of 40 mW [6]. The 455 nm laser was also observed in a cesium vapor by Schultz et al. [7], which was similar to frequency upconversion experiments in rubidium vapor [8]. The high power 455 nm laser source can also be obtained based on the external frequency-doubled amplified semiconductor [Toptica Ltd.] [9], but the linewidth with the order of a few MHz is large in comparison to that of all-solid-state laser systems. In order to achieve the 455 nm laser with high quality, Rong et al. [10] realized pulse narrow-linewidth 455 nm laser by external frequency-doubled Ti:S laser. In this experiment, the external frequency doubler had to be locked to the input laser frequency to obtain stable single-frequency 455 nm laser, which increased the complexity of the laser system. Compared to the external frequency doubler, the intracavity second-harmonic generation (SHG) by inserting a nonlinear crystal into the single-frequency Ti:S laser resonator is an attractive approach to realize the 455 nm output owing to its compact structure and easy realization. With the intracavity doubled Ti:S laser, the SHG of tunable lasers at e.g. 403 nm [11], 423 nm [12] and so on have been developed. Our group obtained a single-frequency 397.5 nm laser by means of the intracavity doubled Ti:S laser and the output power can reach up to 1.58 W and 0.78 W with the intracavity frequency doublers of BIBO (Bismuth Triborate,  $\text{BiB}_3\text{O}_6$ ) and LBO (Lithium Triborate,  $\text{LiB}_3\text{O}_5$ ), respectively [13]. Recently, Demirbas and Baali reported power and efficiency scaling of LD-pumped Cr:LiSAF lasers with the tuning range of 770-1110 nm and frequency doubling to 387-463 nm [14]. So far, there is no study of CW tunable single-frequency and intracavity frequency-doubled Ti:S laser at 455 nm with high output power, to the best of our knowledge. Compared to the single-frequency 397.5 nm laser, it is difficult to achieve a single-frequency 455 nm laser with high output power by intracavity frequency-doubled Ti:S laser. Because the gain of the Ti:S crystal at fundamental-wavelength of 911 nm is 51% lower than that of the peak at 795 nm [15], which increases the threshold pump power and limits the output power of the laser. In order to overcome the disadvantage, we have to design

a new resonator to focus the Gaussian beam waist at Ti:S crystal for decreasing the threshold pump power and enhancing the output power and conversion efficiency of the laser. To develop a desired high power 455.5 nm laser source for special atomic excitation or other applications, in this paper, we firstly investigate the influence of the waist size of the fundamental-wave at the Ti:S crystal on the threshold pump power of the laser when the wavelength of the laser is operated away from the peak gain, and numerically calculate the waist size of the fundamental-wave at the Ti:S crystal when the resonator mirrors with different curvature-radius are employed and its influence on the threshold pump power of the laser. On the base, a compact resonator is designed and built. When a type-I phase-matching BIBO crystal is inserted into the resonator, the single-frequency 455.5 nm laser with the output power up to 421 mW is achieved, the optical-optical conversion efficiency (from 532 nm to 455.5 nm) and long-term power stability are 3.95% and  $\pm 1.5\%$ , respectively. The intensity noise of the laser is measured and reaches the quantum noise limit (QNL) at the frequency of 1.8 MHz. Furthermore, this laser is successfully tuned across the transition  $6^2S_{1/2} \leftrightarrow 7^2P_{3/2}$  of  $^{133}\text{Cs}$  of cesium atoms to resonant excitation of its higher excited state by scanning the optical length of the laser.

## II. CAVITY DESIGN

It has been demonstrated in Ref. [13] that the Ti:S crystal with low concentration and corresponding optimal length often used in the experiment can decrease the absorption of the crystal at the laser wavelength and effectively homogenize the thermal effect of the Ti:S crystal. In order to ensure the oscillation of the 911 nm rather than peak wavelength 795 nm of the Ti:sapphire crystal, the employed cavity mirrors are all coated with high-reflection (HR) films at 911 nm. However, when the Ti:S crystal works at the fundamental wavelength of 911 nm, the measured fractional gain at 911 nm is only 51% of that at 795 nm, which will increase the threshold pump power and limit the output power of the SHG at 455.5 nm. For a CW longitudinal pumped system operating in a fundamental Gaussian beam, the threshold pump power is given by the following equation [16],

$$P_{th} = \frac{1}{\eta_t} \frac{\pi h \nu_p \omega_0^2}{2\sigma\tau} (L_{cav} + L_{xtl})(1 + k^2)[1 - \exp(-\alpha l)]^{-1} \quad (1)$$

where  $\eta_t$  is the transmission efficiency of the pump laser,  $h\nu_p$  is the pump photon energy,  $\sigma$  is the emission cross section which is sensitive to the gain of the fundamental wavelength,  $\tau$  is the upper-state lifetime.  $k$  is the mode size ratio of the pump beam  $\omega_p$  to the laser beam  $\omega_0$ . The final term in brackets represents the pump-absorption efficiency ( $\alpha$  is the absorption coefficient at  $\nu_p$  and  $l$  is the crystal length).  $L_{cav}$  and  $L_{xtl}$  are round-trip cavity loss and the loss caused by the parasitic absorption of the crystal, respectively. The loss caused by the parasitic absorption in the crystal is given by,

$$L_{xtl} = 1 - \exp\left(\frac{-\alpha l_{eff}}{FOM}\right) \quad (2)$$

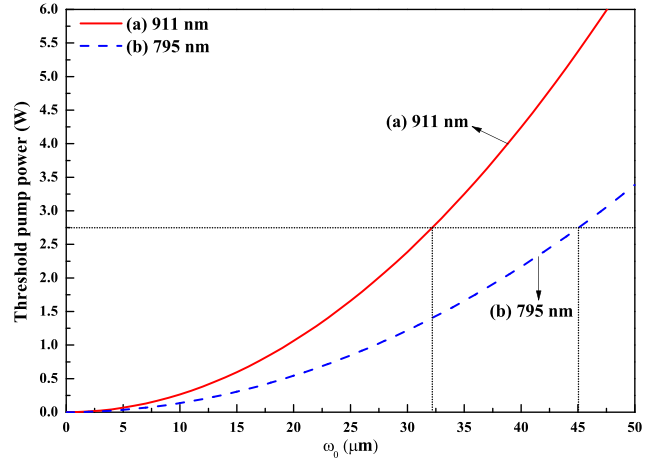


Fig. 1. Dependence of the threshold pump power on the radius of the Gaussian waist at the Ti:S crystal ( $\omega_0$ ).

where  $l_{eff}$  is the effective parasitic absorption length, which equates  $l$  in the travelling-wave cavity.  $FOM$  is the absorption figure of merit defined as the ratio of the absorption at pump laser wavelength to the parasitic absorption at fundamental wavelength.

Substituting Eq. (2) into (1), the relation for the threshold pump power and the mode size  $\omega_0$  at the Ti:S crystal is obtained. Fig. 1 is the function of the threshold pump power of the laser versus the mode size  $\omega_0$  at the Ti:S crystal for the fundamental wavelength of 795 nm and 911 nm, in which the parameters for our laser system,  $\nu_p = c/\lambda_p$ ,  $\lambda_p = 532$  nm,  $\eta_t = 95\%$ ,  $\sigma_{795} = 3.8 \times 10^{-19}$  cm<sup>2</sup>,  $\sigma_{911} = 1.9 \times 10^{-19}$  cm<sup>2</sup>,  $\tau = 3.15$   $\mu$ s,  $L_{cav} = 6\%$ ,  $k = 0.83$  and  $FOM = 200$  are utilized. It is clear that the threshold pump power with the oscillating wavelength of 911 nm is higher than that of 795 nm with the same mode size of the fundamental-wave at the Ti:S crystal. If we want to obtain the same value of the threshold pump power for 911 nm as that for 795 nm, the Gaussian beam waist must be focused by designing a new resonator with small curvature-radius.

Based on above theoretical analysis, a ring resonator consisting of four concave mirrors ( $M_1$ ,  $M_2$ ,  $M_4$  and  $M_5$ ) and two plane mirrors ( $M_3$  and  $M_6$ ) is designed to produce two tight-foci for Ti:S crystal and frequency-doubler, which is shown in Fig. 2. The curvature radii of both  $M_4$  and  $M_5$  are fixed at 50 mm and the length of the laser path outside  $M_1$  and  $M_2$  ( $M_2 \rightarrow M_3 \rightarrow M_4 \rightarrow M_5 \rightarrow M_6 \rightarrow M_1$ ) is kept at 689 mm. In that case, we numerically calculate the waist of the Gaussian fundamental-wave at the Ti:S crystal for three different values of curvature radii of  $M_1$  and  $M_2$  by ABCD matrix, which is shown in Fig. 3. From Fig. 3 we can see when the curvature radii of  $M_1$  and  $M_2$  become from 100 mm to 75 and 50 mm, the radius of the waist at the Ti:S crystal decreases from 43.0  $\mu$ m to 31.7  $\mu$ m and 20.8  $\mu$ m, which are corresponding to the center of the stability range (SR). Substituting these values to Eq. (1), the corresponding threshold pump power decreases from 5.0 W to 2.7 W and 1.17 W, respectively. However,  $M_1$  and  $M_2$  with small curvature radius can also narrow the SR of the laser simultaneously (SR equals to 12.6 mm,

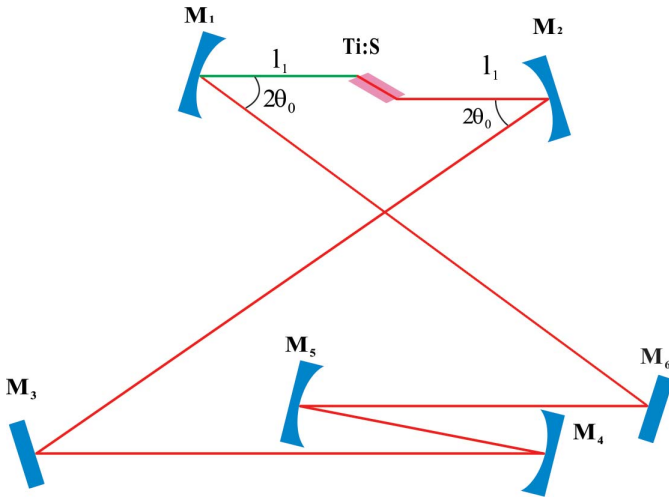
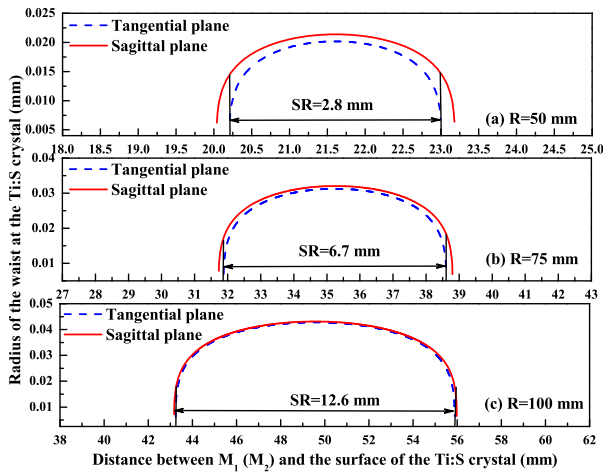


Fig. 2. Configuration of the laser resonator.

Fig. 3. Radius of the waist at the Ti:S crystal and the stability range (SR) for  $M_1$  ( $M_2$ ) with different curvature radius, (a)  $R=50$  mm, (b)  $R=75$  mm, and (c)  $R=100$  mm.

6.7 mm, and 2.8 mm for  $R = 100$  mm, 75 mm and 50 mm, respectively), which will reduce the adaptation of the laser for surrounding environment. Considering the threshold pump power and the SR, a pair of concave mirrors ( $M_1$  and  $M_2$ ) with the curvature radius of 75 mm is employed in the experiment, and the expected threshold pump power is 2.7 W.

### III. EXPERIMENTAL SETUP

To realize a SLM and high efficiency of Ti:S/BIBO laser system, a folded ring resonator with two small waist spots at Ti:S and BIBO crystals is specially designed, which is shown in Fig. 4. The pump source is a single-frequency and frequency-doubled Nd:YVO<sub>4</sub> laser with a maximal 11 W power of the green laser (F-VIII B, Yuguang Co., Ltd) [17]. The pump green laser is coupled into the resonant cavity of the Ti:S laser by a telescope coupling system, which consists of two lenses with the focal lengths of 200 and 100 mm, respectively. A half wave-plate (HWP) in front of the resonator is used for the polarization alignment of the pump laser with

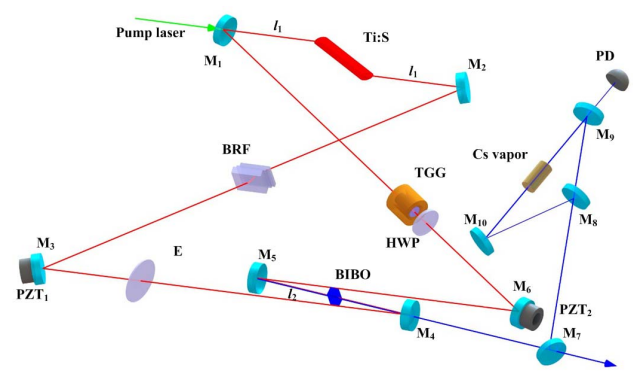


Fig. 4. Experimental setup of the intracavity frequency doubled Ti:S/BIBO laser.

respect to the optical axis of the Ti:S crystal. The resonator of the laser consists of six mirrors (two concave mirrors  $M_1$  and  $M_2$  with curvature radius of 75 mm, two concave mirrors  $M_4$  and  $M_5$  with curvature radius of 50 mm, two flat mirrors  $M_3$  and  $M_6$  both adhered on the PZTs). As an input coupler,  $M_1$  is coated with high transmission (HT) at 532 nm ( $T > 95\%$ ) and HR at 911 nm ( $R > 99.9\%$ ).  $M_2$ ,  $M_3$ , and  $M_6$  are all coated with HR films at 911 nm ( $R > 99.9\%$ ). For output coupling,  $M_4$  is coated with HR films at 911 nm ( $R > 99.9\%$ ) and HT at 455.5 nm ( $T > 95\%$ ) and  $M_5$  is coated with HR films at 911 nm and 455.5 nm ( $R > 99.9\%$ ). The total lengths of the ring cavity are approximate 781 mm with given distances  $l_1 = 35.2$  mm between  $M_1$  and Ti:S crystal and  $l_2 = 51$  mm between  $M_4$  and  $M_5$ . The generated two focused beam waists are  $31.7 \mu\text{m}$  and  $23.3 \mu\text{m}$  for the Ti:S crystal and frequency doubler, respectively. The Brewster-angle-cut ( $60.4^\circ$ ) Ti:S crystal with the dimension of  $\phi 4 \text{ mm} \times 20 \text{ mm}$  and the absorption coefficient of  $0.9 \text{ cm}^{-1}$  at 532 nm is located in the center of  $M_1$  and  $M_2$ , and the c-axis of which is polarized with light propagating direction to its maximal absorption. It is wrapped with indium foil and mounted in a water-cooled copper oven controlled to be  $16.5^\circ\text{C}$ . To compensate the astigmatism resulting from the Brewster-cut Ti:sapphire crystal and the concave mirrors, the folded angles at  $M_1$  and  $M_2$  are set to be  $17.5^\circ$  and the other folded angle at  $M_4$  and  $M_5$  is set to be  $3.5^\circ$  as small as possible [18]. The  $3 \text{ mm} \times 3 \text{ mm} \times 6 \text{ mm}$  nonlinear BIBO crystal, which is coated with antireflection films at both ends for 911 nm and 455.5 nm, is cut at the phase matching angles of  $\theta = 159.4^\circ$ ,  $\varphi = 90^\circ$  for type-I SHG and placed in the center of  $M_4$  and  $M_5$ . The effective nonlinear coefficient for SHG is  $3.32 \times 10^{-12} \text{ m/V}$ . The working temperature of the BIBO crystal is controlled to  $30.85^\circ\text{C}$  by a homemade high-precision temperature controller. The three-plate birefringent filter (BRF) with thickness of 1 mm, 2 mm and 4 mm is inserted into the resonator with its Brewster incidence angle ( $57^\circ$ ) for coarsely frequency-tuning in a broad frequency-band. In order to obtain the stable SLM output laser and realizing finely frequency-tuning of the laser, a thin fused-quartz etalon with the thickness of 0.3 mm is inserted into the resonator. The FSR and the finesse are 333 GHz and 0.6 (for uncoated fused silica), respectively. An optical diode consisting of a  $\phi 4 \text{ mm} \times 8 \text{ mm}$  terbium gallium

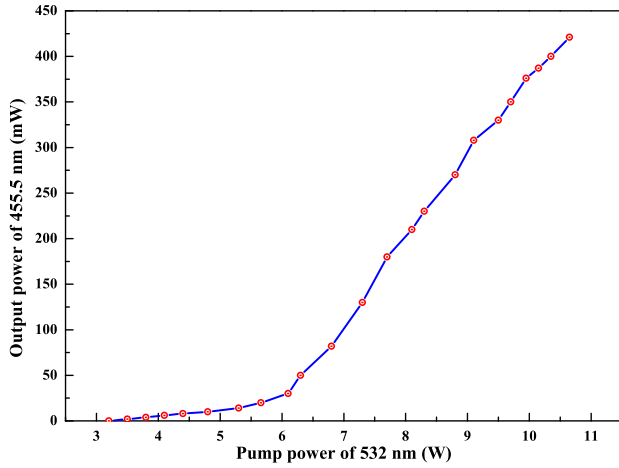


Fig. 5. Output power of 455.5 nm laser versus the incident pump power.

garnet (TGG) rod and an AR-coated zeroth-order HWP at 600 nm-1000 nm is inserted into the cavity to maintain an unidirectional operation. Lastly, a small part of the output laser is separated by  $M_7$  and guided by  $M_8$ ,  $M_9$  and  $M_{10}$  to a  $^{133}\text{Cs}$  atom vapor to scan the saturation absorption spectroscopy and the output signal is recorded by a photodiode (PD) to testing the tuning ability of the laser.

#### IV. EXPERIMENTAL RESULTS

When the frequency doubler of BIBO crystal is inserted into the resonator, the SLM 455.5 nm laser is obtained and the measured output power of SLM 455.5 nm laser as the function of the incident pump power is shown in Fig. 5. It is seen that the threshold pump power is 3.2 W and the output power is up to 421 mW at the pump power of 10.65 W. Correspondingly, the 3.95% maximal conversion efficiency from the pump power (532 nm) to the SHG power (455.5 nm) is achieved. The relatively lower optical conversion efficiency is attributed to the big walk-off angle (about 43.92 mrad) of the BIBO crystal. Because of the imperfect reflection at fundamental wave of the output coupler ( $M_4$ ), about 40 mW fundamental-wave laser can leak along with the blue laser. The measured threshold pump power of 3.2 W is slightly higher than that of the calculated value of 2.7 W is attributable to the imperfect matching between the pump and the fundamental-wave beams. The longitudinal-mode property of the laser system shown in Fig. 6 is measured by a scanned confocal Fabry-Perot (F-P) cavity (F-P-100, Yuguang Co., Ltd.) with the FSR of 750 MHz, which shows that the intracavity frequency doubled Ti:S laser with output wavelength of 455.5 nm can work with SLM operation. That is because the operating point of the laser is located in the region of SLM oscillation when the nonlinear crystal is inserted into the resonator [19]. When the output power of 455.5 nm is 421 mW, we measure the long term stability of the output power for 3 hours, the fluctuation of which is less than  $\pm 1.5\%$ , as shown in Fig. 7. The beam quality of the obtained blue laser is measured by a  $M^2$  meter (M2SET-VIS, thorlabs), and the values of  $M_x^2$  and  $M_y^2$  are 1.23 and 1.92, respectively. The intensity

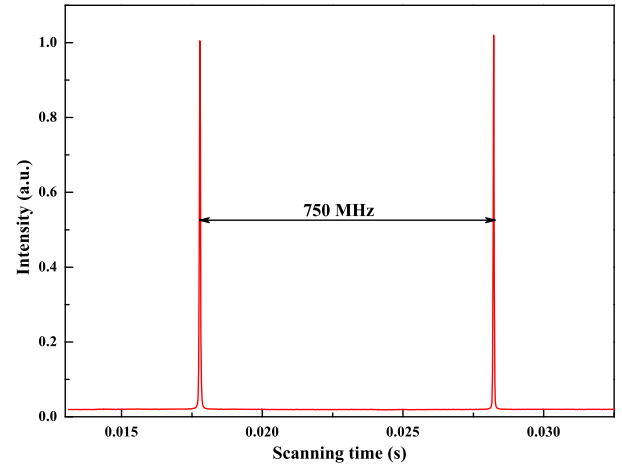


Fig. 6. Longitudinal-mode structure of the laser by scanning the confocal F-P cavity.

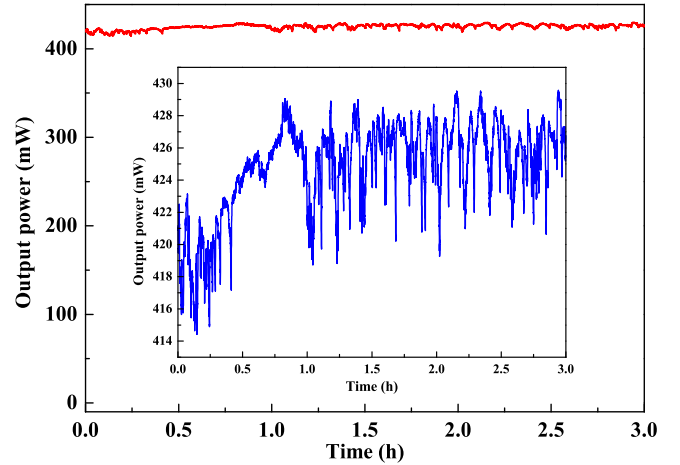


Fig. 7. Long term power stability of 455.5 nm laser for 3 h.

noise is measured by a homemade self-homodyne-detector (YG-BHD02, Yuguang Co., Ltd.) which includes two silicon photo-diodes (PD, S3399) [20]. The common mode rejection ratio of the used self-homodyne-detector is 34 dB, which is high enough to satisfy the requirement for implementing measurement. The optical signals detected by two PDs are amplified by the integrated amplifiers (ADA 4817) and then the amplified photo currents of two PDs are combined with a negative or positive power combiner (+/-). The sum and the subtract photocurrents stand for the intensity noise and the corresponding quantum noise limit (QNL) [21], respectively. Finally, the noise spectra of the sum (subtract) photo currents are analyzed by a spectral analyzer with the resolution bandwidth (RBW) of 30 kHz and the video bandwidth (VBW) of 30 Hz. The measured intensity noise shown in Fig. 8 depicts that the intensity noise of the 455.5 nm laser reaches the QNL almost at the 1.8 MHz.

In order for precisely tuning the wavelength of the laser to 455.528 nm at desired transition of  $6^2S_{1/2} \leftrightarrow 7^2P_{3/2}$  of Cesium atoms, the wavelength of the fundamental-wave is coarsely tuned near 911 nm by rotating BRG. Then controlling the

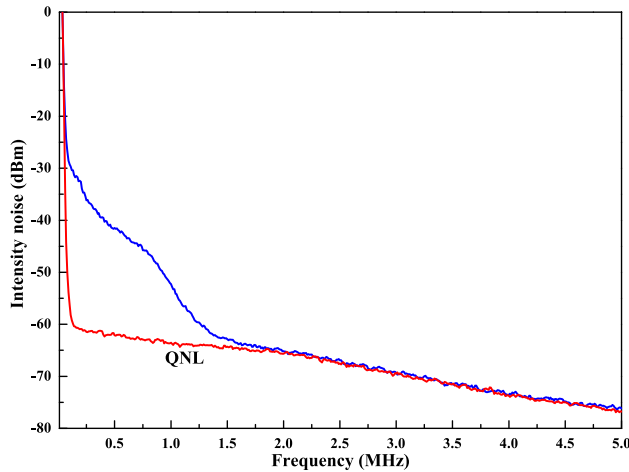


Fig. 8. Measured intensity noise of the single-frequency 455.5 nm laser.

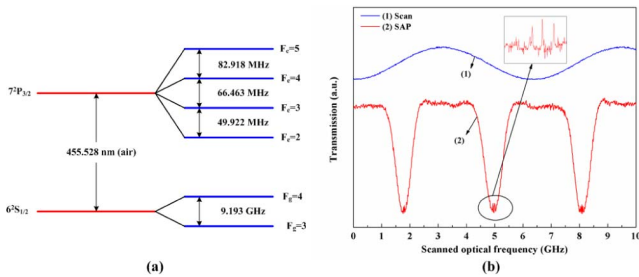


Fig. 9. (a) Relative energy levels of Cesium; (b) Saturation absorption spectrum of Cesium.

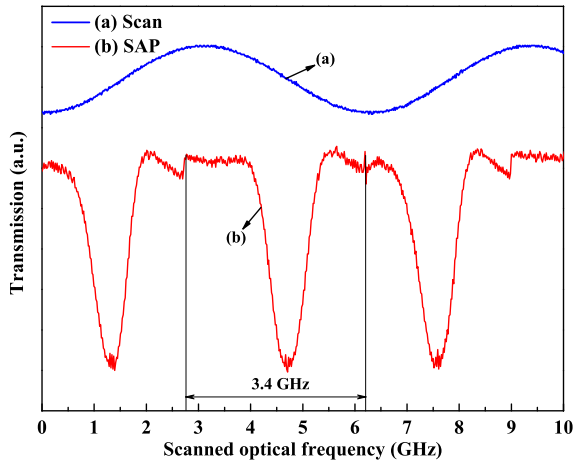


Fig. 10. Scanning range up to 3.4 GHz of the laser.

position angle and working temperature of E can finely get the laser wavelength at 911.05 nm. The precisely tuning of the laser frequency is further realized by adjusting the cavity optical length via PZTs adhered on  $M_3$  or  $M_6$  mirrors. The SAS (in the dip of red line in Fig.9(b)) of the higher-state hyperfine transitions  $6^2S_{1/2}(F_g = 4) \leftrightarrow 7^2P_{3/2}(F_e = 3, 4, 5)$  of cesium (the energy levels shown in Fig. 9(a)) is obtained when the laser is continuously tuned up to 3.4 GHz before the occurrence of a mode-hopping in Fig. 10. The continuously tuning range of 3.4 GHz is larger than a FSR of the laser

because of the existence of the nonlinear loss introduced by the nonlinear BIBO crystal [22]. Over 3 GHz, the six peaks in inset of Fig. 9(b) are corresponding to principal and cross-over lines of  $F_g = 4 \leftrightarrow F_e = 3$ ,  $F_g = 4 \leftrightarrow F_e = 3, 4$ ,  $F_g = 4 \leftrightarrow F_e = 4$ ,  $F_g = 4 \leftrightarrow F_e = 3, 5$ ,  $F_g = 4 \leftrightarrow F_e = 4, 5$ , and  $F_g = 4 \leftrightarrow F_e = 5$ . In the process of the frequency-tuning, the power fluctuation is too small to be ignored.

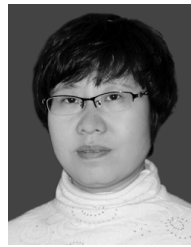
## V. CONCLUSION

In summary, we have realized a tunable single-frequency 455.5 nm laser by means of intracavity frequency-doubled Ti:S laser. Since the gain of the fundamental wavelength of 911 nm is lower than that the peak 795 nm, which will increase the threshold pump power of the laser, we have optimized the curvature radii of the resonator mirrors to focus the waist of the fundamental-wave beam at the Ti:sapphire crystal and decrease the threshold pump power. Considering the threshold pump power and the SR of the laser, the mirrors with curvature radius of 75 mm are used in the experiment and a high power, CW tunable SLM Ti:S/BIBO laser system with the output wavelength of 455.5 nm is obtained. The output power is up to 421 mW from the pump power of 10.65 W all-solid state laser at 532nm with the optical conversion efficiency of 3.95%. The intensity noise of the 455.5 nm laser reaches the QNL almost at the 1.8 MHz. Because of the existence of the nonlinear BIBO crystal, the continuously tuning range up to 3.4 GHz is achieved by adjusting the cavity optical length of the resonator. Lastly, the obtained laser system is successfully applied to scan the SAS of transitions  $6^2S_{1/2} \leftrightarrow 7^2P_{3/2}$  of  $^{133}\text{Cs}$  atoms around the wavelength of 455.5 nm. The wavelength of 455.5 nm laser is also corresponding to the transition of  $^{138}\text{Ba}^{2+}$  ion, therefore it is important for cooling and trap of atoms and ions, and for other applications such as excitation of quantum dot, superconductor materials, nonlinear optics, quantum manipulation and computing.

## REFERENCES

- [1] K. F. Wall, "Blue light sources based on Ti:sapphire lasers," in *Imag. Appl. Opt., OSA Tech. Dig. (CD)*, paper LWA2, pp. 1–3, 2011.
- [2] C. Auchter, T. W. Noel, M. R. Hoffman, S. R. Williams, and B. B. Blinov, "Measurement of the branching fractions and lifetime of the  $5D_{5/2}$  level of  $\text{Ba}^+$ ," *Phys. Rev. A*, vol. 90, no. 6, p. 060501-1–060501-3, Dec. 2014.
- [3] M. Auzinsh, R. Ferber, F. Gahbauer, A. Jarmola, L. Kalvans, and A. Atvars, "Cascade coherence transfer and magneto-optical resonances at 455 nm excitation of cesium," *Opt. Commun.*, vol. 284, no. 12, pp. 2863–2871, Jun. 2011.
- [4] D.-W. Wang, S.-Y. Zhu, J. Evers, and M. O. Scully, "High-frequency light reflector via low-frequency light control," *Phys. Rev. A*, vol. 91, p. 011801(R), Jan. 2015.
- [5] M. P. Le Flohic, J. Y. Allain, G. M. Stéphan, and G. Mazé, "Room-temperature continuous-wave upconversion laser at 455 nm in a  $\text{Tm}^{3+}$  fluorozirconate fiber," *Opt. Lett.*, vol. 19, no. 23, pp. 1982–1984, 1994.
- [6] M. Schmidt, E. Heumann, C. Czeranowsky, and G. Huber, "Generation of 455 nm radiation by intracavity doubling of a Nd:LiLuF4 laser," in *Conf. Lasers Electro-Opt., OSA Tech. Dig.*, paper CThC1, pp. 387–388, 2001.
- [7] J. T. Schultz *et al.*, "Coherent 455 nm beam production in a cesium vapor," *Opt. Lett.*, vol. 34, no. 15, pp. 2321–2323, 2009.
- [8] T. Meijer, J. D. White, B. Smeets, M. Jeppesen, and R. E. Scholten, "Blue five-level frequency-upconversion system in rubidium," *Opt. Lett.*, vol. 31, no. 7, pp. 1002–1004, 2006.

- [9] [Online]. Available: [http://www.toptica.com/products/research\\_grade\\_diode\\_laser/frequency\\_converted\\_diode\\_laser/dl\\_shg\\_pro\\_frequency\\_doubled\\_tunable\\_diode\\_laser.html](http://www.toptica.com/products/research_grade_diode_laser/frequency_converted_diode_laser/dl_shg_pro_frequency_doubled_tunable_diode_laser.html)
- [10] S. Rong, X. Zhu, and W. Chen, "All-solid-state narrow-linewidth 455-nm blue laser based on Ti:sapphire crystal," *Chin. Opt. Lett.*, vol. 7, no. 1, pp. 43–45, 2009.
- [11] R. T. White *et al.*, "Tunable single-frequency ultraviolet generation from a continuous-wave Ti:sapphire laser with an intracavity PPLN frequency doubler," *Appl. Phys. B*, vol. 77, no. 6, pp. 547–550, Nov. 1988.
- [12] L. S. Cruz and F. C. Cruz, "External power-enhancement cavity versus intracavity frequency doubling of Ti:sapphire lasers using BIBO," *Opt. Exp.*, vol. 15, no. 19, pp. 11913–11921, 2007.
- [13] H. Lu, X. Sun, J. Wei, and J. Su, "Intracavity frequency-doubled and single-frequency Ti:sapphire laser with optimal length of the gain medium," *Appl. Opt.*, vol. 54, no. 13, pp. 4262–4266, 2015.
- [14] U. Demirbas and I. Baali, "Power and efficiency scaling of diode pumped Cr:LiSAF lasers: 770–1110 nm tuning range and frequency doubling to 387–463 nm," *Opt. Lett.*, vol. 40, no. 20, pp. 4615–4618, 2015.
- [15] P. F. Moulton, "Spectroscopic and laser characteristics of Ti:Al<sub>2</sub>O<sub>3</sub>," *J. Opt. Soc. Amer. B*, vol. 3, no. 1, pp. 125–133, 1986.
- [16] J. Harrison, A. Finch, D. M. Rines, G. A. Rines, and P. F. Moulton, "Low-threshold, cw, all-solid-state Ti:Al<sub>2</sub>O<sub>3</sub> laser," *Opt. Lett.*, vol. 16, no. 8, pp. 581–583, 1991.
- [17] Q. Yin, H. Lu, and K. Peng, "Investigation of the thermal lens effect of the TGG crystal in high-power frequency-doubled laser with single frequency operation," *Opt. Exp.*, vol. 23, no. 4, pp. 4981–4990, 2015.
- [18] Y. Sun, H. D. Lu, and J. Su, "Continuous-wave, single-frequency, all-solid-state Ti:Al<sub>2</sub>O<sub>3</sub> laser," *Acta Sinica Quantum Opt.*, vol. 14, no. 3, pp. 344–347, 2008.
- [19] H. Lu, J. Su, Y. Zheng, and K. Peng, "Physical conditions of single-longitudinal-mode operation for high-power all-solid-state lasers," *Opt. Lett.*, vol. 39, no. 5, pp. 1117–1120, 2014.
- [20] H. J. Zhou, W. H. Yang, Z. Li, X. Li, and Y. Zheng, "A bootstrapped, low-noise, and high-gain photodetector for shot noise measurement," *Rev. Sci. Instrum.*, vol. 85, no. 1, p. 013111, 2014.
- [21] H. P. Yuen and V. W. S. Chan, "Noise in homodyne and heterodyne detection," *Opt. Lett.*, vol. 8, no. 3, pp. 177–179, 1983.
- [22] H. Lu, X. Sun, M. Wang, J. Su, and K. Peng, "Single frequency Ti:sapphire laser with continuous frequency-tuning and low intensity noise by means of the additional intracavity nonlinear loss," *Opt. Exp.*, vol. 22, no. 20, pp. 24551–24558, 2014.



**Fengqin Li** was born in 1977. She received the Ph.D. degree in physics from Shanxi University, Taiyuan, China, in 2012.

She is currently a Researcher with the Institute of Opto-Electronics, Shanxi University. Her current research interests include all-solid-state laser technology, quantum optics devices, and tunable optics devices.



**Huijuan Li** was born in 1989. She received the B.S. degree in physics from Xinzhou Normal College, Xinzhou, China, in 2013.

She is currently pursuing the master's degree in optics with the Institute of Opto-Electronics, Shanxi university. Her current research interests include single-frequency lasers and nonlinear optics.



**Huadong Lu** was born in 1981. He received the Ph.D. degree in laser technology from Shanxi University, Taiyuan, China, in 2011.

He is currently an Associate Professor with the Institute of Opto-Electronics, Shanxi University. His current research interests include all-solid-state laser technology, quantum optics devices, and tunable optics devices.